2000

Conducting Polymers and Corrosion III. A Scanning Vibrating Electrode Study of Poly(3-octyl pyrrole) on Steel and Aluminum

J. He
North Dakota State University, USA

V. J. Gelling
North Dakota State University, USA

D. E. Tallman
North Dakota State University, USA

G. P. Bierwagen
North Dakota State University, USA

G G. Wallace
University of Wollongong, gwallace@uow.edu.au

Journal of The Electrochemical Society, **147** (10) 3667-3672 (2000)
S0013-4651(00)01-029-6 CCC: $7.00 © The Electrochemical Society, Inc.

Conducting Polymers and Corrosion
III. A Scanning Vibrating Electrode Study of Poly(3-octyl pyrrole) on Steel and Aluminum

Jie He,[a] Victoria Johnston Gelling,[a] Dennis E. Tallman,[a,*,z] Gordon P. Bierwagen,[b,*] and Gordon G. Wallace[c]

[a]*Department of Chemistry and* [b]*Department of Polymers and Coatings, North Dakota State University, Fargo, North Dakota 58105, USA*
[c]*Intelligent Polymer Research Institute, Department of Chemistry, University of Wollongong, Wollongong, New South Wales 2522, Australia*

Electroactive conducting polymers (ECPs) continue to be of considerable interest as components of corrosion-resistant coating systems. ECPs, in addition to being conductive, are redox active materials, typically with potentials that are positive of iron and aluminum. Thus, as with chromate, interesting and potentially beneficial interactions of ECPs with active metal alloys such as steel and aluminum are anticipated. In this work, the scanning vibrating electrode technique (SVET), also known as the current density probe, was used to probe such interactions between a poly(3-octyl pyrrole) coating (POP) and cold-rolled steel and aluminum (Al 2024-T3) substrates. The POP coatings were scribed to simulate a defect through the coating to the metal substrate surface. The SVET was used to map the current flowing in and around the defect while the sample was immersed in either 3% NaCl (steel) or in dilute Harrison solution (aluminum), an aqueous solution consisting of 0.35% $(NH_4)_2SO_4$, 0.05% NaCl. Although there were significant differences in the behavior of the POP-coated steel and POP-coated aluminum substrates, both exhibited a significant delay before the onset of any observable current compared to uncoated or epoxy-coated samples. Current density maps for the steel clearly indicate that the reduction reaction occurred on the conducting polymer surface, with oxidation confined to the defect. Current density maps for the aluminum alloy never displayed significant oxidation at the defect. Rather, reduction (after a significant delay) occurred at the defect as well as across the polymer surface, with concomitant localized undercoating oxidation of the aluminum substrate.

Manuscript submitted January 10, 2000; revised manuscript received June 19, 2000.

There is increasing interest in the use of electroactive conducting polymers (ECPs) as components of corrosion-resistant coating systems, either directly as a primer coating or surface treatment, or as a component blended with more conventional coatings.[1] In part, this interest in ECPs is motivated by the desire to find suitable replacements for chromate-based coatings, currently used for corrosion control of iron and aluminum alloys.[2,3] Such use of chromate is under intense scrutiny due to environmental issues and health concerns surrounding its use.[3,4] ECPs, in addition to being conductive, are redox active materials, typically with potentials that are positive of iron and aluminum.[1] Thus, as with chromate, interesting and potentially beneficial interactions of ECPs with active metal alloys such as steel and aluminum are anticipated, with concomitant alteration of their corrosion behavior.

Following Deberry's[5] work on the corrosion-protective properties of polyaniline on stainless steel, many papers have been published describing corrosion studies of conducting polymers on various active metals.[1] Most of the work reported to date has involved polyaniline, either on steel[6-16] or on aluminum.[17-21] There have been fewer reports of corrosion studies involving polypyrrole on active metals, the majority of these studies involving films that were electrochemically deposited onto steel.[22-27] There appears to be little or no reported work involving polypyrrole on aluminum alloys.

One of the challenges in developing conducting polymer coatings in general, and polypyrrole coatings in particular, has been to overcome the difficulty in processing these materials. The general lack of solubility and fusibility of these materials make the formation of coatings on active metals difficult. As noted previously, direct electrochemical deposition of the ECP coating can be used, but this approach is not straightforward with active metals that oxidize at the deposition potential. One successful approach to improving the processibility of polypyrrole has been to add an organic substituent to the pyrrole ring that improves the solubility of the polymer in common organic solvents,[28,29] permitting a coating of the polymer to be directly cast onto an active metal.

Our laboratory has been investigating the corrosion protective properties of poly(3-octyl pyrrole) (or POP) coatings on aluminum 2024-T3 alloy. Long-term immersion tests (*ca.* 2 years) indicate that this polymer with a polyurethane topcoat performs better than a chromated-epoxy primer with a polyurethane topcoat.[30] The work described in this report was undertaken in order to understand better the interaction between POP and active metals.

In a companion paper,[31] we reported on the use of the scanning vibrating electrode technique (SVET), also known as the current density probe (CDP), to probe the current flowing in and around a defect introduced into a chromated-epoxy primer on steel and on aluminum. In this work, the SVET was used to probe interactions between a POP coating and cold-rolled steel and aluminum (Al 2024-T3) substrates. The POP coatings were scribed to simulate a defect through the coating to the metal substrate surface. The SVET was used to map the current flowing in and around the defect while the sample was immersed in either 3% NaCl (steel) or in dilute Harrison solution (aluminum).

Experimental

Sample preparation.—The poly(3-octyl pyrrole) was synthesized electrochemically by the Intelligent Polymer Research Institute (Wollongong, Australia) and contained perchlorate and paratoluene sulfonate counterions. The synthetic details and polymer characterization have been described previously.[29] Briefly, the polymer was generated galvanostatically at a platinum electrode at a current density of 1 mA/cm^2 from a solvent mixture of CCl_4 (80%) and CH_2Cl_2 (20%) containing 0.1 M monomer (3-octyl pyrrole), 0.1 M tetrabutylammonium perchlorate, and 0.025 M tetrabutylammonium *p*-toluenesulfonate. The soluble fraction of the electrosynthesized polymer was recovered from the liquor and excess electrolyte[29] removed. Cast films of the polymer were both electroactive (by cyclic voltammetry) and conductive (*ca.* 5×10^{-3} S/cm by the four-point probe technique).[29]

* Electrochemical Society Active Member.
z E-mail: dtallman@plains.nodak.edu

S0013-4651(00)01-029-6 CCC: $7.00

The cold-rolled steel (Q-Panel), aluminum alloy (Al 2024-T3, Q-Panel), and pure aluminum (99.998%, Alfa Aesar) substrates were first polished using 600 grit silicon carbide, washed with hexane, and air-dried. After this pretreatment, the POP coating was applied by solution casting from a 1% solution in a solvent consisting of 50% CCl_4 and 50% CH_3CN. The coatings were allowed to dry overnight. The average coating thickness was 2.3 ± 1.6 μm. No topcoat was employed in this study.

Control samples were prepared by coating steel and aluminum substrates with a plain epoxy coating, a polymer of epichlorohydrin and bisphenol A (Dow Chemical D.E.R. 331) with Ancamide 2353 curing agent (Air Products). The average coating thickness for the plain epoxy coating was 30 ± 8.5 μm. This polymer is electrically insulating and redox inactive, thus providing a basis for assessing the influence of the ECP on the corrosion behavior of the substrates. The results of these control experiments are described in more detail in the companion paper.[31]

Instrumentation and experimental conditions.—The SVET instrumentation used in these experiments was from Applicable Electronics (Forestdale, MA) and is described in detail elsewhere.[31,32] Scanning electron microscopy (SEM) and energy-dispersive X-ray (EDX) analysis of Al 2024-T3 samples were performed with a JEOL JSM-6300V microscope (JEOL, Ltd., Tokyo, Japan) equipped with a Noran Voyager II EDX analysis system (Madison, WI). An accelerating voltage of 15 kV, a take-off angle of 29.0°, and a 100 s count were used.

Samples were prepared for SVET measurement by cutting into 1 × 1 cm squares and masking by a Polyester 5 adhesive tape (3M Company) such that only a 2 × 2 mm square opening of the sample was exposed. The POP coating of each sample was scribed to introduce a defect extending to the metal surface, the area of the defect ranging from 0.1 to 0.3 mm^2 (epoxy-coated control samples were scribed in the same manner). The sample was mounted in a Teflon sample cell and the appropriate immersion solution (*ca.* 5 mL) was added. The immersion solution for the Al 2024-T3 samples was dilute Harrison solution (0.35% $(NH4)_2SO_4$, 0.05% NaCl in H_2O). The immersion solution for the cold-rolled steel samples was 3% NaCl solution. These solutions were prepared from reagent-grade salts and distilled water.

Scans were initiated within 5 min of immersion and were collected every 20 min for the duration of the experiment, typically 20 h. Each scan consisted of 400 data points obtained on a 20 × 20 grid, with an integration time of 1 s per point. A complete scan required 10 min, followed by a 10 min rest period prior to the next scan. The current density maps are displayed in two ways. In one method, the normal or *z* component of the measured current density in the plane of the vibrating electrode is plotted in 3D format over the scan area, with positive and negative current densities representing anodic and cathodic regions, respectively. In the other method, vectors representing current density magnitude and direction are superimposed on an optical image of the immersed sample. In all cases, the bottom edge of the optical micrograph corresponds to the *x* axis of the 3D plot. The measurements were taken at the open-circuit potential. At least six specimens of each sample type were prepared and scanned to assess reproducibility of the observed phenomena. In each case, representative scans are presented.

Results and Discussion

Poly(3-octyl pyrrole) coating on steel.—There are rather striking similarities between the results obtained in this work with the POP coating on steel and the results reported for a chromated-epoxy coating on steel.[31] As was observed with the chromated-epoxy coating, the POP coating delayed the onset of corrosion within the defect. However, the delay was significantly longer, typically *ca.* 3 h with the POP coating, compared to *ca.* 40 min for the chromated epoxy coating, and virtually no delay for a plain epoxy coating.[31] Figure 1 (top) shows the current density map for POP-coated steel at 5 min immersion in 3% NaCl (the optical micrograph for this sample is displayed in Fig. 2). No significant current flow was observed and similar inactivity was maintained for *ca.* 3 h. Figure 1 (bottom) shows the map recorded at 166 min immersion, at which time the first significant current flow was observed. The current increased with time, reaching the maximum (*ca.* 100 (A/cm^2) after 5 h and 35 min immersion (Fig. 2). The current then slowly decreased as the defect became covered with a dark deposit of corrosion product, reaching near background levels after *ca.* 19 h. As observed for a chromated epoxy coating (but in contrast to a plain epoxy coating),[31] the corrosion product appeared to be adherent, with little or no suspended corrosion product evident in the immersion solution.

In these experiments, the current associated with the defect is always anodic, with two main anodic sites for this particular sample apparent in the current maps of Fig. 2. Significant cathodic current was never observed within the defect. Rather, the cathodic current was always distributed more or less uniformly across the conducting polymer surface, as clearly evident from Fig. 2. We postulate that oxygen reduction occurs at the POP/electrolyte interface, with electron transfer from the metal to oxygen being mediated by the POP. This process drives the oxidation reaction observed in the defect, which ultimately leads to passivation of the exposed metal within the defect. Of course, the oxidizing potential of POP may be an important factor in this mediation process. Kinlen and co-workers[33] recently reported a similar observation for polyaniline-coated steel where the scanning reference electrode technique revealed localized anodes in pinhole defects and a delocalized cathode spread over the polyaniline surface.

POP coating on Al 2024-T3.—The results obtained for POP on Al 2024-T3 are particularly interesting. In the initial experiments, the defects introduced into the coatings were of dimensions similar to those used for the steel samples (for example, see Fig. 2). However,

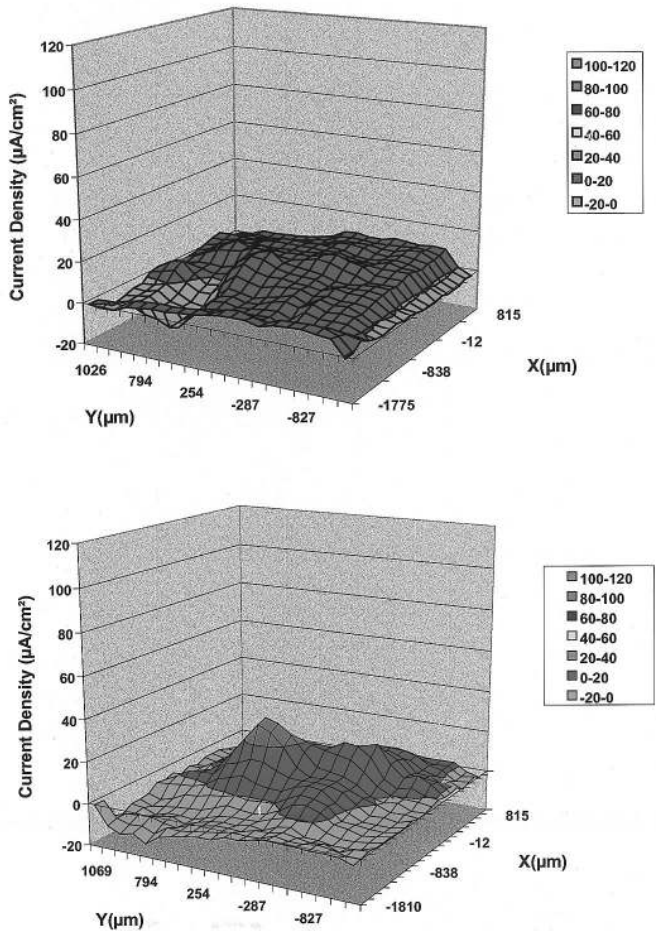

Figure 1. Current density maps for POP on steel immersed in 3% NaCl (3D representation of the *z* component of the current density): (top) at 5 min immersion and (bottom) at 2 h and 46 min immersion. The optical micrograph of this sample is shown in Fig. 2.

S0013-4651(00)01-029-6 CCC: $7.00

little or no activity was observed with these samples even after many hours of immersion, so the size of the defect was increased. Figure 3 illustrates a typical sample with the larger defect, this optical micrograph and current density map captured at the 5 min mark. Close examination of the current density map reveals a very small oxidation current flowing at the defect, particularly noticeable at the left edge of the defect, corresponding to the left end of the *x* axis and the midpoint of the *y* axis. A correspondingly small reduction current occurs at coated areas of the substrate. Admittedly these currents are near the background level, but may reflect the development of a protective oxide coating at the defect during the early stages of immersion. Even with this rather sizable defect, the current flow typically remained at near background level for over 22 h. By comparison, sizable current flow (>10 $\mu A/cm^2$) was observed at chromated-epoxy coatings within *ca.* 5 h and at plain epoxy coatings within *ca.* 20 min.

The first significant current flow at this sample was observed after 22 h, 14 min of immersion, shown in Fig. 4 (top). However, in contrast to other combinations of coatings and metals we have examined where oxidation always occurred at the defect, the oxidation current in this case appeared to originate at a coated area of the aluminum alloy. The current increased over the next hour during which time the defect area exhibited a rather uniform reduction current (Fig. 4). Indeed, from this time of immersion onward, oxidation at the defect was never observed with these samples. The metal within the defect remained shiny throughout the immersion experiment with no visual evidence of corrosion products. To assess the reproducibility of this observation, a total of eight POP-coated samples were examined by the SVET. In every case, this general behavior was observed, with no significant oxidation occurring at the defect of any of the eight samples. Additionally, there appeared to be no coating defects (*e.g.,* pinholes) that might account for the observed behavior.

The oxidation current observed in Fig. 4 continued to increase over the next several hours, reaching the level shown in Fig. 5 (top) after 26 h, 34 min immersion. The optical micrograph of Fig. 5 (bottom) confirms that the oxidation is occurring at a coated region of the alloy and not at the defect. The current continued to flow for several days, dropping to *ca.* 20 $\mu A/cm^2$ after 5 days, at which point the experiment was terminated and the coating removed by dissolving in chloroform followed by acetone.

The oxidation currents observed in Fig. 4 and 5 indicate that anions were moving into (or equivalently, cations out of) the POP coating. There are at least two possible explanations for this observation: either the POP coating itself was oxidized or the aluminum alloy beneath the coating was oxidized. An optical micrograph of the Al 2024-T3 surface after removal of the POP coating is shown in Fig. 6. The POP coating has been removed from the 2×2 mm scan area, but not from the surrounding area protected by the Polyester 5 tape. Visible within this scan area is the original defect (the scribe mark). Also visible (and much more apparent under binocular observation) are pits formed in the alloy surface at the site of the oxidation current (compare the micrographs of Fig. 5 and 6). Thus, we conclude that the observed oxidation current was due to the oxidation of the aluminum alloy (*i.e.,* pitting corrosion) beneath the POP coating.

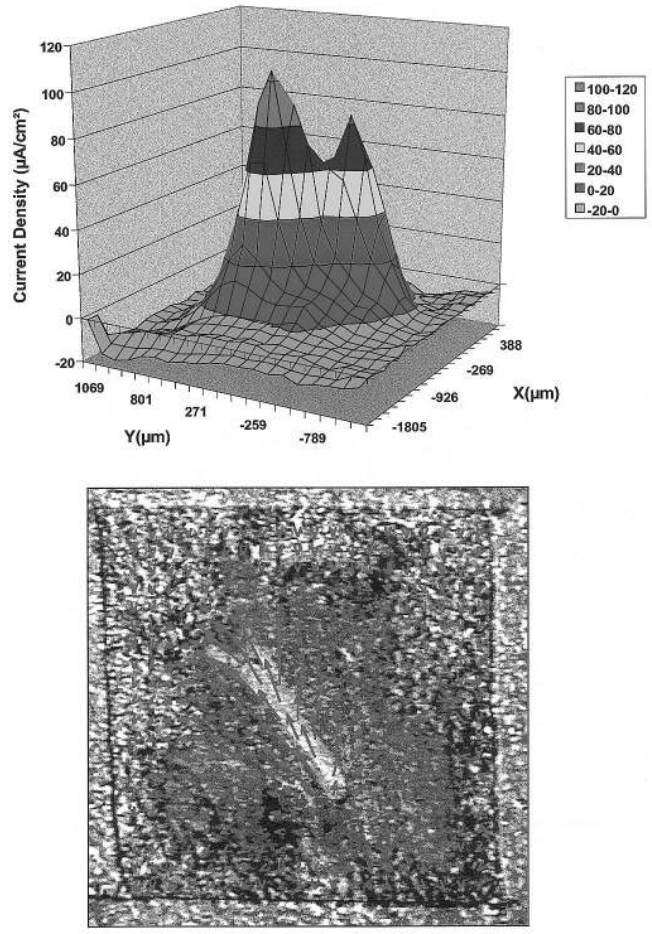

Figure 2. Current density maps for POP on steel after 5 h and 35 min immersion in 3% NaCl: (top) 3D representation of the *z* component of the current density and (bottom) optical micrograph of the sample with current density vectors superimposed.

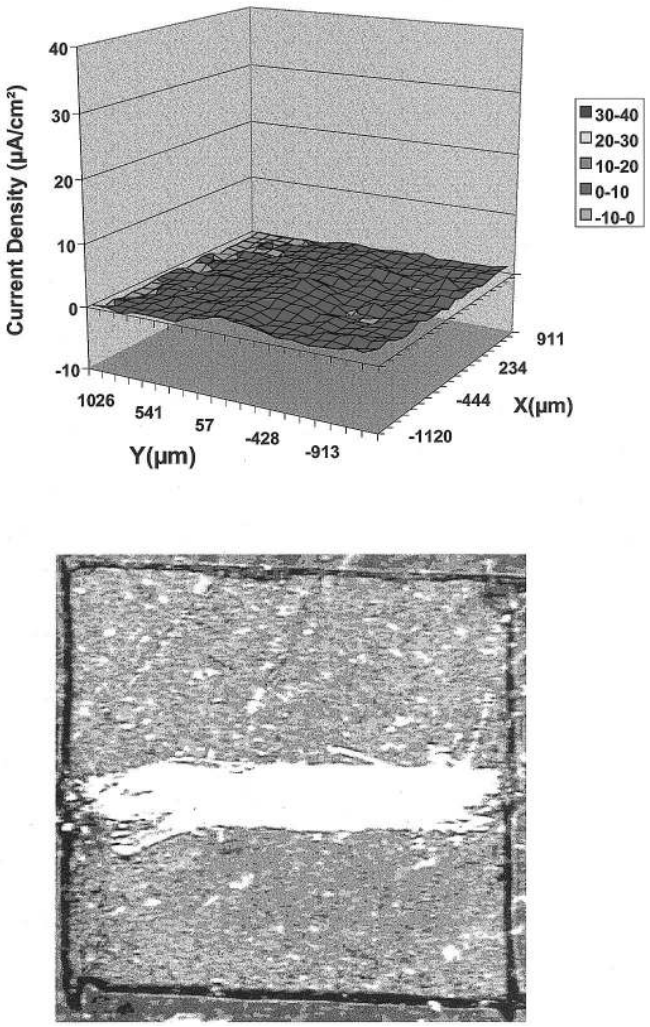

Figure 3. Current density map and optical micrograph for POP on Al 2024-T3 immersed in dilute Harrison solution: (top) 3D representation of the *z* component of the current density at 5 min immersion and (bottom) optical micrograph of sample with current vectors omitted for clarity.

S0013-4651(00)01-029-6 CCC: $7.00

There remains a confounding question. Why does the oxidation of aluminum alloy always occur under the polymer coating and not at exposed metal within the defect as observed for steel? After all, the defect area is exposed directly to the aggressive electrolyte ions, whereas the POP-coated area is not (although exchange of the POP counterions with electrolyte ions likely occurs). One explanation might involve direct oxidation of the metal by the POP with concomitant reduction of the POP. However, such an internal redox reaction would not require charge compensation of the POP from the electrolyte (*i.e.,* there would be no ion flux at the POP surface) and such a process would not be observed by the SVET. The POP coating may mediate the oxidation of the alloy by shuttling electrons from the alloy to oxygen (or other oxidant) at the POP/electrolyte interface, as observed for steel (Fig. 2). Indeed, reduction at the POP/electrolyte interface (as well as in the defect) was often observed with the Al alloy (*e.g.,* see Fig. 7). However, the mediation of electron transfer by the POP would not explain the absence of oxidation within the defect and the localized undercoating oxidation.

One possible explanation is that the POP provided a thermodynamic assist to the oxidation of the aluminum alloy by forming stable metal ion complexes with the oxidized metal ions (principally Al^{3+} and/or Cu^{2+}). Indeed, a similar mechanism has been suggested for polyaniline on Al 2024-T3, where X-ray photoelectron spectroscopy showed depletion of Cu from the alloy surface by the conducting polymer.[34] As the metal ions enter the POP, charge balance would be maintained by an anion flux from electrolyte into the polymer, resulting in the observed current flow above the polymer surface. A slight color change in the POP coating immediately above and around the site of oxidation was observed (from black to dark blue-green), indicating a localized change in coating composition

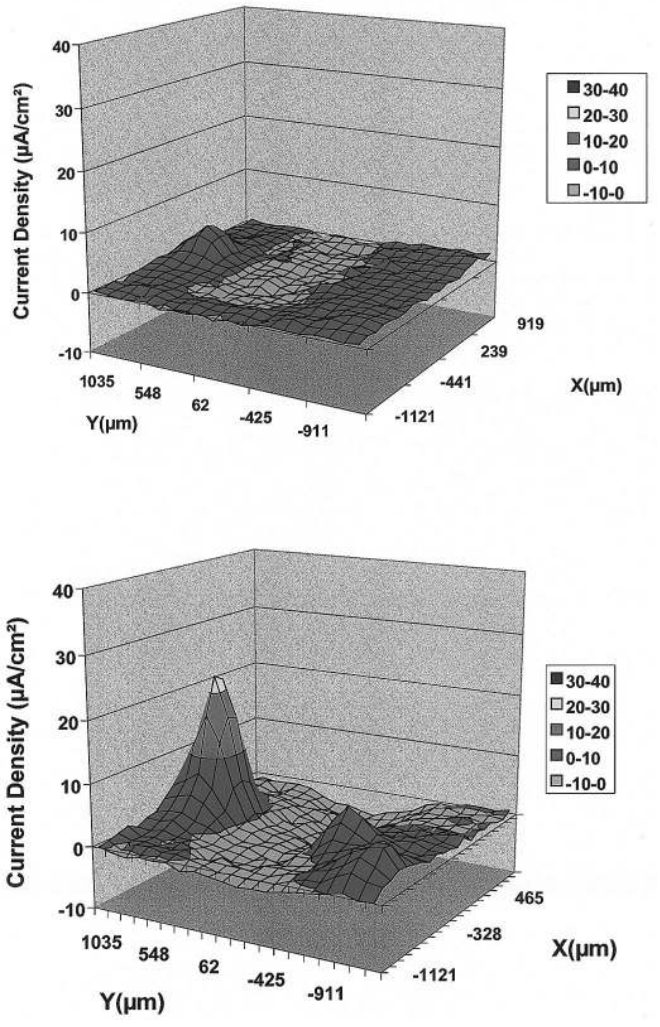

Figure 4. Current density maps for POP on Al 2024-T3 immersed in dilute Harrison solution (3D representation of the *z* component of the current density): (top) at 22 h, and 14 min immersion and (bottom) at 23 h, 14 min immersion.

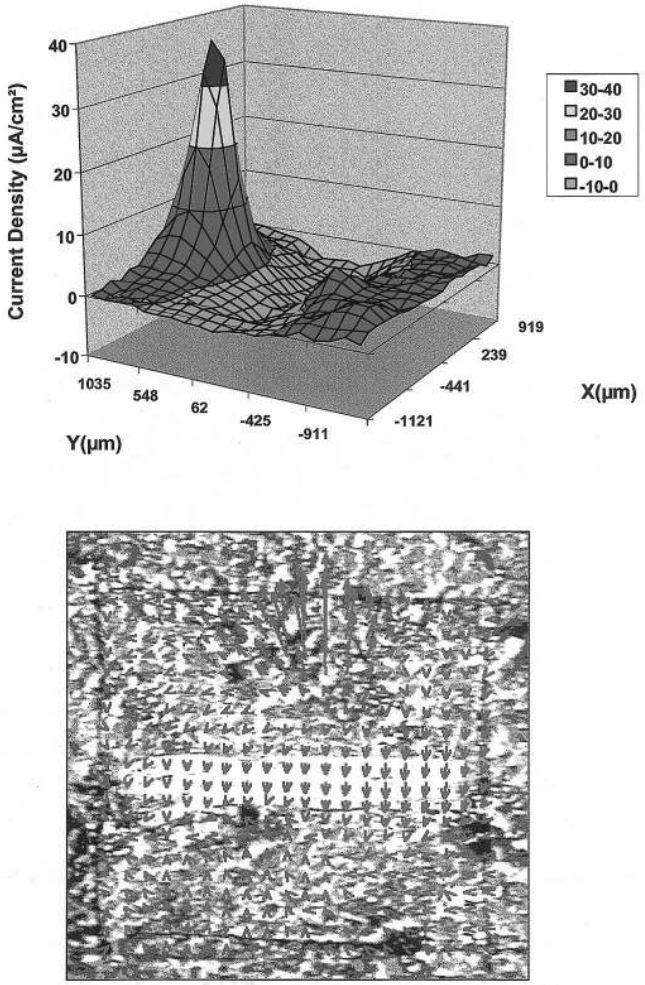

Figure 5. Current density maps for POP on Al 2024-T3 immersed in dilute Harrison solution: (top) 3D representation of the *z* component of the current denstiy at 26 h, and 34 min immersion and (bottom) optical micrograph of sample with current density vectors superimposed.

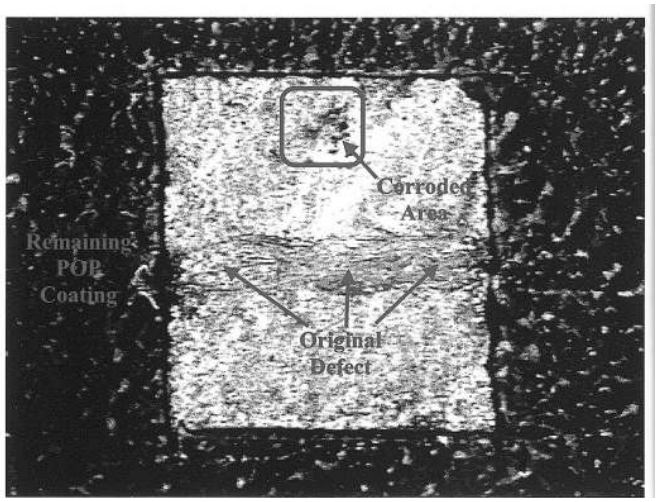

Figure 6. Optical micrograph of the sample from Fig. 5 after removal of the POP coating, showing the region of undercoating pitting corrosion.

S0013-4651(00)01-029-6 CCC: $7.00

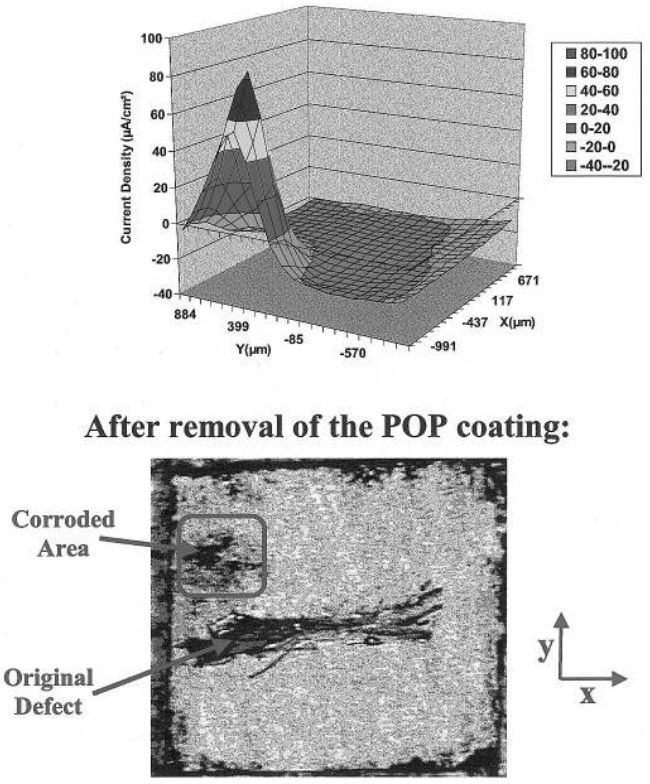

Figure 7. (Top) current density map for POP on Al 2024-T3 immersed in dilute Harrison solution and (bottom) optical micrograph of the sample after removal of the POP coating.

consistent with this hypothesis. Furthermore, the incorporation of metal ions into polypyrrole by complexation has been reported, both by direct coordination to the pyrrole nitrogen[35] and by incorporation and strong binding (as counterions) of anionic metal complexes.[36]

EDX analysis.—All POP-coated Al 2024-T3 alloy specimens examined by SVET eventually displayed (after the previously described induction period) localized undercoating corrosion, as exemplified by Fig. 5 and 6. Such a localized oxidation process may be related to the known heterogeneous structure of the aluminum alloy surface. In particular, the inhomogeneous distribution of Cu in the alloy microstructure (intentionally developed to optimize mechanical properties of the alloy) is known to be responsible for the low pitting resistance of the alloy.[37,38] In an attempt to address this question, EDX analysis was performed on selected samples. Figures 7 and 8 show a typical result. Note in Fig. 7 that (as observed previously in Fig. 5 and 6) the oxidation was highly localized and resulted in a visible pit after coating removal. However, unlike the result of Fig. 5 where the reduction reaction was confined largely to the defect area, the reduction process in Fig. 7 was distributed rather uniformly across both the defect and the polymer.

Figure 8 shows scanning electron micrographs of the sample of Fig. 7. Seven regions are labeled on the micrographs: A, B, and C in the scribe area; D and E in defect-free regions; and F and G in the pit area. The copper content of each of these regions is reported in Table I. The "mass effect" may render these analytical results semiquantitative at best,[39] and the actual Cu content in the Cu-rich regions may be higher than that reported in Table I. It is clear from these results that the site where the pitting occurred is a Cu-rich site, containing well above the 4-5% average Cu content expected for this alloy.

While we cannot assign a specific phase to the Cu-rich regions F and G, the most common such phase for this alloy is reported to be the S phase particles (Al_2CuMg), comprising approximately 60% of particles greater than 0.5-0.7 μm and covering approximately 2.7% of the alloy surface.[40] Furthermore, S phase particles are active relative to the aluminum matrix phase and are reported to undergo partial dissolution by dealloying.[40] Such active regions are likely candidates for the site of oxidation observed in the SVET experiments. The Cu content of S phase particles is *ca.* 45% and increases as a result of dealloying.[40] Our observation of only *ca.* 20% Cu in regions F and G suggests that Cu is preferentially removed from these particles, perhaps a consequence of its ability to complex with the conducting polymer as noted previously.

The second most abundant Cu-rich phase in the alloy is $Al_{24}Cu_2FeMn$, comprising approximately 12.3% of all particles and covering approximately 0.85% of the surface.[40] These particles are among the largest found on the alloy surface[40] and contain *ca.* 14% Cu. The Cu contents observed in regions F and G are larger than this (20%), suggesting that if these particles were responsible for the observed oxidation process, then dealloying leading to an enrichment in Cu must have occurred. However, no Fe or Mn was detected in these regions, whereas some Mg was observed (though less than 1%). This supports the notion that the Cu-rich regions are S phase particles.

POP coating on pure Al metal.—If a Cu-rich phase(s) of the Al 2024-T3 alloy is responsible for the highly localized oxidation currents observed with POP-coated alloy, then a somewhat different result might be expected for experiments conducted on pure aluminum metal. Figure 9 shows current density maps for POP-coated Al (99.998%). As observed with the alloy, there was a significant time delay before the onset of any observable current, at which point only reduction was observed in the defect area. However, in contrast to the alloy where the oxidation current was always very localized, the oxidation current on pure Al appeared to be much more distributed across the substrate surface. In particular, the current appeared primarily around the perimeter of the exposed area, as distant from the defect as possible (Fig. 9). When the coating was removed, no pitting was observed and no visible corrosion products remained on the Al surface. Instead, the surface was shiny, suggesting a rather uniform oxidation of the aluminum surface, most likely producing Al^{3+} ions which were incorporated into (or perhaps transported through) the coating. Further experiments are planned to elucidate the details of this process. Nevertheless, these observations support the notion that Cu-rich regions in the alloy are responsible for the localized oxidation current observed with the POP-coated Al 2024-T3.

Conclusions

Poly(3-octyl pyrrole) coatings on cold-rolled steel and on aluminum 2024-T3 alloy have the ability to delay the onset of corrosion within a defect. In this regard, the POP coatings are similar to chro-

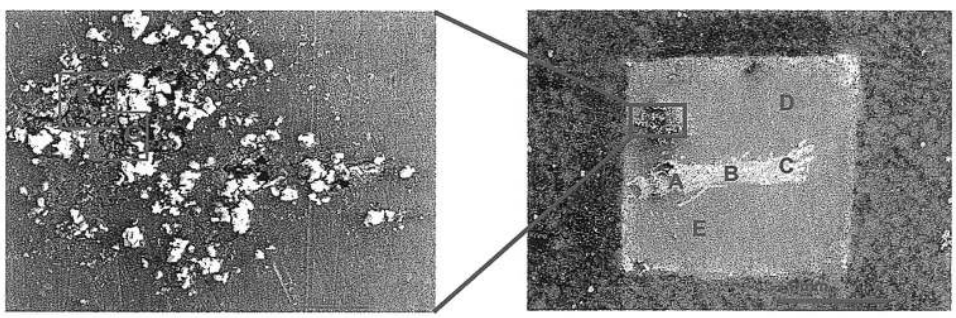

Figure 8. Scanning electron micrograph of the sample of Fig. 7 after removal of the POP coating showing the entire scan region (right; bar = 1 mm) and a magnified view of the pit region (left; bar = 100 μm). The letters denote regions of EDX analysis (see Table I).

S0013-4651(00)01-029-6 CCC: $7.00

Table I. Copper content in designated region of Fig. 8.

Region	A	B	C	D	E	F	G
Cu (wt %)	5.6	8.5	11.2	4.0	5.2	20.5	20.7

mated-epoxy coatings, but produce even longer delays before the onset of current flow in and around the defect. The defect apparently is protected by a mechanism involving formation and/or stabilization of a passive layer in the defect, likely a consequence of the ability of these coatings to render the surface potential within the defect more positive (noble). Eventually, however, the aggressive immersion medium breaches the passive layer and corrosion commences. At this point, the behaviors of steel and of aluminum differ.

On cold-rolled steel, oxidation is observed within the defect and reduction occurs rather uniformly across the conducting polymer surface. The oxidation within the defect is sustained for a significantly longer period of time than observed with an inert (plain epoxy) coating and leads to a more adherent corrosion product, features also observed with a chromated-epoxy coating.

On Al 2024-T3, significant oxidation current is never observed within the defect, only reduction current, and only then after a significant delay from the time of initial immersion. The oxidation process appears to involve removal of metal from copper-rich regions of the alloy surface beneath the POP coating. This oxidation does not appear to be driven by the conducting polymer, but rather it is coupled to the reduction process occurring in the defect and, in some cases, also over the POP surface. The polymer may provide a thermodynamic assist to the process through metal ion complexation or metal ions may be simply transported through the coating to the electrolyte. Further experiments are planned to help elucidate these details.

Acknowledgments

This work was supported by the Air Force Office of Scientific Research, grant no. F49620-96-1-0284 and F49620-97-1-0376 (AASERT), North Dakota State University. We are grateful to Dr. Chee O. Too and Dr. Syed A. Ashraf of the Intelligent Polymer Research Institute (University of Wollongong, Australia) for synthesis of the poly(3-octyl pyrrole) used in this work.

North Dakota State University assisted in meeting the publication costs of this article.

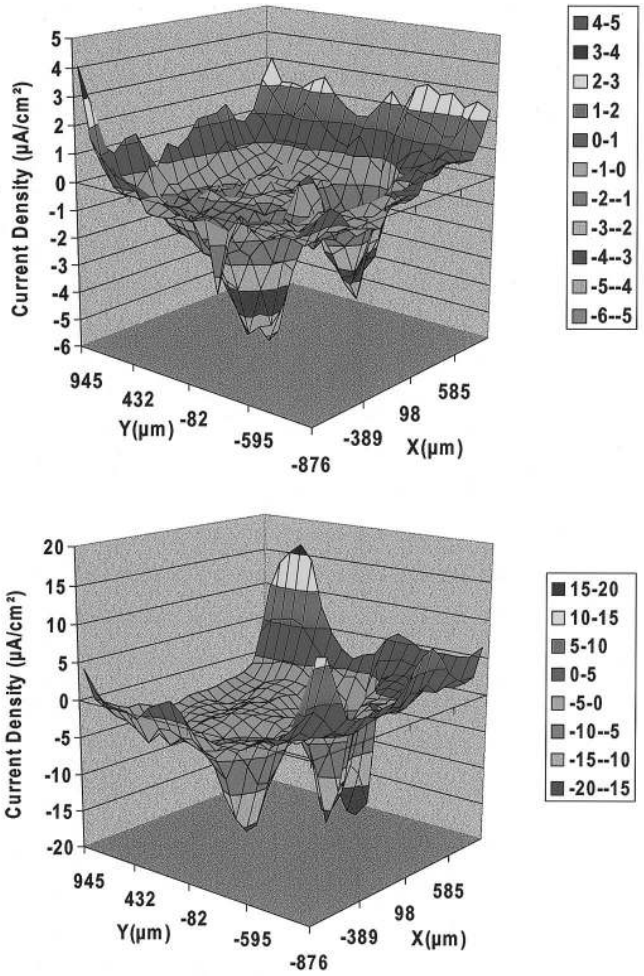

Figure 9. Current density maps for POP on pure (99.998%) Al metal immersed in dilute Harrison solution at (top) 8.6 h immersion and (bottom) at 12.6 h immersion.

References

1. W-K. Lu, S. Basak, and R. L. Elsenbaumer, *Handbook of Conducting Polymers,* 2nd ed., T. A. Skotheim, R. L. Elsenbaumer, and J. R. Reynolds, Editors, p. 881, New York (1998).
2. I. M. Zin, R. L. Howard, S. J. Badger, J. D. Scantlebury, and S. B. Lyon, *Prog. Org. Coat.,* **33,** 203 (1998).
3. S. M. Cohen, *Corrosion,* **51,** 71 (1995).
4. EPA Federal Register, *National Emission Standards for Hazardous Air Pollutants for Source Categories: Aerospace Manufacturing and Rework Facilities,* **60**(170), p. 45947, Sept 1, 1995.
5. D. W. Deberry, *J. Electrochem. Soc.,* **132,** 1022 (1985).
6. W. K. Lu, R. L. Elsenbaumer, B. Wessling, *Synth. Met.,* **71,** 2163 (1995).
7. N. Ahmad and A. G. MacDiarmid, *Synth. Met.,* **78,** 103 (1996).
8. K. G. Thompson, C. J. Bryan, B. C. Benicewicz, and D. A. Wrobleski, *ACS Polym. Preprints,* **35,** 265 (1994).
9. M. Fahlman, S. Jasty, and A. J. Epstein, *Synth. Met.,* **85,** 1323 (1997).
10. J. R. Santos, Jr., L. H. C. Mattoso, and A. J. Motheo, *Electrochim. Acta,* **43,** 308 (1998).
11. A. Talo, O. Forsén, and S. Yläsaari, *Synth. Met.,* **102,** 1394 (1999).
12. B. Wessling and J. Posdorfer, *Synth. Met,,* **102,** 1400 (1999).
13. M-C. Bernard, A. Hugot-LeGoff, S. Joiret, N. N. Dinh, and N. N. Toan, *Synth. Met.,* **102,** 1383 (1999).
14. M-C. Bernard, C. Deslouis, T. El Moustafid, A. Hugot-LeGoff, S. Joiret, and B. Tribollet, *Synth. Met.,* **102,** 1381 (1999).
15. I. Kulszewicz-Bajer, M. Zagórska, A. Bany, and L. Kwiatkowski, *Synth. Met.,* **102,** 1385 (1999).
16. D. E. Tallman, Y. Pae, and G. P. Bierwagen, *Corrosion,* **55,** 779 (1999).
17. R. J. Racicot, R. L. Clark, H-B. Liu, S. C. Yang, M. N. Alias, and R. Brown, *Proc. SPIE-Int. Soc. Opt. Eng.,* **2528,** 251 (1995).
18. R. J. Racicot, R. L. Clark, H-B. Liu, S. C. Yang, M. N. Alias, and R. Brown, *Mater. Res. Soc. Symp. Proc.,* **413,** 529 (1996).
19. A. J. Epstein, J. A. O. Smallfield, H. Guan, and M. Fahlman, *Synth. Met.,* **102,** 1374 (1999).
20. D. E. Tallman, Y. Pae, and G. P. Bierwagen, *Corrosion,* **56**, 401 (2000).
21. R. J. Racicot, S. C. Yang, and R. Brown, *Corrosion,* **531,** 1 (1997).
22. F. Beck and R. Michaelis, *J. Coat. Technol.,* **64,** 59 (1992).
23. A. Ferreira, S. Aeiyach, J. J. Aaron, and P. C. Lacaze, *Electrochim. Acta,* **41,** 1801 (1996).
24. N. V. Krstajic, B. N. Grgur, S. M. Jovanovic, and M. V. Vojnovic, *Electrochim. Acta,* **42,** 1685 (1997).
25. B. N. Grgur, N. V. Krstajic, M. V. Vojnovic, C. Lacnjavac, and Lj. Gajic-Krstajic, *Prog. Org. Coat.,* **33,** 1 (1998).
26. J. Reut, A. Öpik, and K. Idla, *Synth. Met.,* **102,** 1392 (1999).
27. C. A. Ferreira, S. Aeiyach, A. Coulaud, and P. C. Lacaze, *J. Appl. Electrochem.,* **29,** 259 (1999).
28. J. Y. Lee, D. Y. Kim, and C. Y. Kim, *Synth. Met.,* **74,** 103 (1995).
29. S. A. Ashraf, F. Chen, C. O. Too, and G. G. Wallace, *Polymer,* **37,** 2811 (1996).
30. V. Johnston Gelling, D. E. Tallman, G. P. Bierwagen, and G. G. Wallace, *Prog. Org. Coat.,* (2000), Accepted for publication.
31. J. He, V. Johnston Gelling, D. E. Tallman, and G. P. Bierwagen, *J. Electrochem. Soc.,* **147,** 3661 (2000).
32. C. Scheffey, *Rev. Sci. Instrum.,* **59,** 787 (1988).
33. P. J. Kinlen, V. Menon, and Y. Ding, *J. Electrochem. Soc.,* **146,** 3690 (1999).
34. A. J. Epstein, J. A. O. Smallfield, H. Guan, and M. Fahlman, *Synth. Met.,* **102,** 1374 (1999).
35. M. B. Inoue, K. W. Nebesny, Q. Fernando, Ma. M. Castillo-Ortega, and M. Inoue, *Synth. Met.,* **38,** 205 (1990).
36. A. Deronzier and J-C. Moutet, *Coord. Chem. Rev.,* **147,** 339 (1996).
37. A. Garner and D. Tromans, *Corrosion,* **35,** 55 (1979).
38. G. S. Chen, M. Gao, and R. P. Wei, *Corros. Sci.,* **52,** 8 (1996).
39. J. I. Goldstein, D. E. Newbury, P. Echlin, D. C. Joy, and E. Lifshin, *Scanning Electron Microscopy and X-Ray Microanalysis,* p. 339, Plenum Press, New York (1981).
40. R. G. Buchheit, R. P. Grant, P. H. Hlava, B. McKenzie, and G. L. Zender, *J. Electrochem. Soc.,* **144,** 2621 (1997).